Uniaxial Extension of End-Linked Polystyrene Networks Containing Deuterated Free Chains Studied by Small-Angle Neutron Scattering: Effect of the Network Chains and the Size of the Free Chains

A. Ramzi,*,† A. Hakiki,‡ J. Bastide,‡ and F. Boué†

Laboratoire Léon Brillouin (CEA-CNRS), Centre d'Etudes, Saclay, F-91191 Gif-sur-Yvette Cedex, France, and Institut Charles Sadron (CRM-EAHP), 6 rue Boussingault, F-67083 Strasbourg Cedex, France

Received September 4, 1996; Revised Manuscript Received February 5, 1997[⊗]

ABSTRACT: We have studied end-linked polystyrene networks containing labeled (deuterated) free chains subjected to an uniaxial deformation using small-angle neutron scattering (SANS). The networks are made by end-linking protonated polystyrene precursor chains of a narrow size distribution. As for statistical networks investigated earlier, the isointensity lines on the bidimensional detector have the double-winged shape known as "butterfly patterns". They appear as a figure "8" at small values of the scattering vector, **q**, oriented along the stretching direction, corresponding to a larger scattering in the parallel than in the perpendicular direction even at $q \rightarrow 0$. We relate the existence of butterfly patterns to preexisting heterogeneities in the cross-linking density, which cause spatial fluctuations of the free chain concentration. Such heterogeneities are therefore present even in end-linked networks. They can be attributed to imperfect chemistry or to more physical origins: heterogeneity in the spatial distribution of entanglement or the presence of large loops.

1. Introduction

For many years, small-angle neutron scattering (SANS) has been used in order to study polymer networks such as dense rubbers (dry networks) or swollen rubbers (gels). Regarding the uniaxial extension of a *statistical* network made of nonlabeled chains randomly cross-linked containing a small proportion of *un-cross-linked labeled (deuterated) chains* of the same species, a totally unexpected phenomenon has been observed.[1−3] At low values of the momentum transfer q, the scattering intensity increases strongly with the elongation ratio λ for **q** vectors parallel to the stretching direction. Conversely, in the direction perpendicular to the elongation axis, the scattering intensity decreases slightly for small elongation ratios and then remains approximately constant when λ is further increased. This anomaly is especially striking when considering the isointensity contours on a bidimensional detector. Before stretching, these contours are of course circular. After the strain is applied, they are transformed at low q into some kind of double-winged pattern, having the shape of an "8" called "*butterfly*".[3] The long axis of these patterns is oriented parallel to the stretching axis, contrary to what is expected from isolated objects being stretched. One would have in this case elliptical patterns with a long axis perpendicular to the stretching. The phenomenon was shown to be due to interchain correlations (i.e., correlations between two different chains).[4] The concentration fluctuations of labeled chains are enhanced along the parallel direction, but not along the perpendicular one. A simple classical theory based on linear elasticity predicts that the fluctuations of the mobile species inside a stretched network decrease along the stretching axis, leading to butterfly patterns with the axis joining the centers of the lobes perpendicular to the stretching (called "normal" butterflies).[5] Similar patterns were observed more than 20 years ago by Inoue et al., for microphase-separated triblock copolymers[6] and recently in the case of sheared semidilute solutions by light scattering[7,8] and SANS,[9] but it has not been established that they have the same origin.

Theoretically, different models were proposed to understand the physical origins of butterfly patterns. We shall compare them to our experimental data. In the first model,[10,11] the frozen fluctuations, invisible in the preparation state, are revealed by swelling or stretching. In other words, the spatial separation of the "hard" regions (more cross-linked) from the "soft" regions (less cross-linked) is responsible for the formation of concentration fluctuations at large scales. The second model is based on the concentration dependence of the elastic modulus and the coupling between the deformation and concentration fields. According to this model, a strong enhancement of thermal fluctuations in the direction parallel to the stretching axis is observed in "soft" elastic two-component solids subjected to a uniaxial deformation.[12] Finally, Onuki has recently proposed a model based on the perturbation treatment of uncorrelated frozen heterogeneities.[13]

Recently, SANS experiments on statistical networks[1,2] containing mobile deuterated chains allowed us to make detailed comparisons with these models. We concluded that only the third model could give a sensible description (although only qualitative) of the progressive variation of the scattering with the elongation ratio λ. Similar conclusions were obtained from the scattering of swollen statistical networks subjected to stretching (the solvent is taken as the mobile species).[14] Such networks were randomly cross-linked, justifying the assumption of a heterogeneous cross-link density.

Here, we consider a different system, where cross-linking should in principle be more "*regular*": each precursor chain is short and linked by the two ends. The chemistry chosen here is, in principle, well controlled.

* To whom correspondence should be addressed. Present address: DSM Research, Dept. PAC, Postbus 18, NL-6160 MD, Geleen, The Netherlands

† Centre d'Etudes.

‡ Institut Charles Sadron.

⊗ Abstract published in *Advance ACS Abstracts,* April 1, 1997.

S0024-9297(96)01309-5 CCC: $14.00 © 1997 American Chemical Society

Table 1. Characteristics of the Different End-Linked Networks

sample	M_{WH}[a]	M_{WD}[b]	Q_{eq}[c]
RBH1	5720		7.80
RBH2	10200		10.20
RBH3	15500		12.00
RBH11	5720	12000	7.20
RBH12	10200	12000	8.30
RBH13	15500	12000	10.50
RBH21	5720	73000	8.70
RBH22	10200	73000	10.50
RBH23	15500	73000	11.40

[a] Molecular weight of precursors. [b] Molecular weight of labeled chains. [c] Equilibrium swelling ratio.

The same molecular weights of free chains as those inside the statistical networks are used, and we also use similar average cross-linking ratios.

2. Experimental Details

2.1. Preparation of Networks and Co-Trapping of the Deuterated Chains. Polystyrene (PS) networks were prepared in two steps. The first consists of the synthesis of linear polystyrene chains (precursors) by anionic polymerization of the styrene at low temperatures (−70 °C) as described by Richards and Szwarc.[15] The advantage of this technique is the weak polydispersity of the polymers so obtained. The second step involves the linking of the precursor chains exclusively through functional groups placed at their two ends. When the reactions are carried nearly to completion, the resulting materials are urethane networks. These can be called "model networks"[16,17] because (i) the average molecular weight M_c of the network chains is known (being equal to the number-average molecular weight M_n of the precursor chains), (ii) the functionality of the junction points is known (being equal to that of the cross-linking agent), and (iii) the method of preparation is assumed to ensure a weak incidence of network imperfections (loops and dangling ends).

Synthesis of the Precursor. The solvent used in experiments (tetrahydrofuran, THF) was purified by distillation. The styrene was initially dried on calcium chloride, distilled over sodium wire under reduced pressure, and then stored under argon immediately before use. In a 2 L flask maintained under argon atmosphere, the THF was first cooled using an ice−2-propanol mixture. The quantity of solvent was adjusted in order to obtain a concentration of styrene of 10% by weight. At a temperature of −40 °C, three droplets of the initiator (Naphthalene−potassium) were added with stirring in order to neutralize the protonic impurities. The mixture was brought to −70 °C. After 1 h of stirring, the styrene and the initiator were successively added. The molecular weight of the desired polymer is controlled by the quantity of the initiator. At the end of the polymerization reaction, the ends of the obtained chains can be neutralized for later use by adding a small quantity of methanol. Alternately, in order to obtain the precursor, the ends are transformed into hydroxyl groups by the addition of an excess of ethylene oxide (4−6 times the stoichiometric quantity) into the reaction flask at low temperature under rapid stirring.

The resulting mixture was then kept at −20 °C for a period of 12H in order to assure the completeness in the formation of the hydroxyl groups. After this time, the reaction was neutralized by the addition of a small amount of acid chloride (HCl), filtered and precipitated twice in methanol. The polymer was then dried at 50 °C in a vacuum desiccator. Table 1 summarizes the main characteristics of the different polymers.

End-Linking. The networks were prepared from the OH-terminated PS precursors in semidilute solution. The chains are end-linked by trifunctional junctions, using tris(isocyanato-4)phenyl thiophosphate (DRF) as a cross-linking agent by means of diazobicyclootane (DABCO) as catalyst.[18] The concentration of polymer in the solution was 27% by weight (close to $c^* = 200M_w^{-0.8}$ for $M_{WH} = 5720$). The mixture, which appeared homogeneous, was poured into a mold in an atmosphere of argon and kept at 50 °C for several days. The resulting gel was dried, initially at room temperature and then, under vacuum, by gently increasing the temperature up to 150 °C. The equilibrium swelling of the samples, Q_{eq}, was measured after drying.

Deuterated chains were included inside the networks (made of nondeuterated chains) as had been done previously for statistical networks.[1,2] The deuterated chains of molecular weight M_{WD} were added during the end-linking reaction but remain free in the gel because their functional ends were neutralized before use. One can check that they may be extracted by solvent washing. Their presence during the formation of the network influences weakly the equilibrium swelling ratio Q_{eq}. The latter varies only with the molecular weight M_{WH} of the precursor in a systematic way: as is usually observed, Q_{eq} decreases when increasing the cross-linking density. The values of Q_{eq} and the characteristics of the different samples are listed in Table 1. The volume fraction ϕ_D of the incorporated labeled chains is equal to 8.65% in the dry state for all samples.

Deformation and Stress−Strain Measurements. Samples having dimensions of approximately 7 cm × 1 cm × 0.1 cm were cut from each dried network. They were immersed in a silicone oil bath, allowed to equilibrate to a temperature T = 134 °C, i.e. T_g + 34 °C (T_g is the glass transition temperature for polystyrene). Then they were stretched rapidly from an initial length L_0 to a final length $L_f = \lambda L_0$. They were maintained at a constant shape and temperature for a time t_R[19] (the relaxation time) and finally quenched by taking them out of the bath. The samples were observed by small-angle neutron scattering (SANS) in this frozen state. After the measurement, they were dipped again in the bath under extension at the same temperature, 134 °C, stretched at a higher λ, relaxed for 10 min, quenched, observed again by SANS, and so on. Simultaneously, the equilibrium force f_{eq} was measured after 10 min for each elongation. The equilibrium values of the reduced stress G is given by[20−23]

$$G = f_{eq}/l_f e_f (\lambda^2 - \lambda^{-1}) \quad (1a)$$

$$= \sigma/(\lambda^2 - \lambda^{-1}) \quad (1b)$$

where l_f and e_f are the width and the thickness of the sample after stretching, and $\sigma = f_{eq}/l_f e_f$ is the true stress which represents the force per unit area measured in the strained state. The elongation, λ, was increased step by step (with one SANS measurement per step) from 1 to λ_{break}, at which the sample breaks in a time shorter than 10 min.

Small-Angle Neutron Scattering. Small-angle neutron scattering measurements were performed at the spectrometer PAXY of the Laboratoire Léon Brillouin. The experimental procedure has already been described.[1] The detector is bidimensional with 128 × 128 cells (5 × 5 mm^2 each). The distance between the detector and the sample was D = 3.2 m, and the wavelength of the incident neutron beam used was W = 10 Å, giving the momentum transfer $q = (4\pi/W)(\sin(\theta/2))$ (θ is the scattering angle) between 7×10^{-3} and 7×10^{-2} Å^{-1}. In the case of stretched samples, the scattering was anisotropic. The cells corresponding to the same modulus q of the scattering vector **q** are regrouped inside sectors of 20 and 15° (parallel and perpendicular respectively) to the elongation axis (in the isotropic state, the regrouping of the data was annular). In order to correct for detector efficiency, the raw data are normalized by the scattering of a 1 mm water sample used as a standard. Subtraction of the normalized pure hydrogenated polystyrene intensity eliminates the incoherent background and yields the coherent scattering cross section in absolute units (cm^{-1}) denoted $I_{iso}(q)$, $I(q_{||})$ or $I(q_\perp)$. On a map of the detector, one can also draw isointensity curves joining all cells of approximately equal number of neutron counts.

3. Experimental Results

3.1. Mechanical Measurements. In this section, we discuss data for the tensile stress σ under deforma-

tion for the samples observed using SANS. The results are compared to data for the same kind of networks, but without free chains present. Note that the goal of this study is not only to perform the mechanical characterization of the samples but also to check the effect on the networks of the free species inside them. The stress−strain data were interpreted in terms of the "reduced stress" or modulus defined by eq 1. The equilibrium values of G were plotted against reciprocal elongation ($1/\lambda$), as suggested by the semiempirical equation of Mooney and Rivlin[24,25]

$$G = 2C_1 + 2C_2/\lambda \tag{2}$$

in which $2C_1$ and $2C_2$ are constants independent of λ. Thus the value of the modulus is $2C_1$ in the limit of large deformation ($\lambda^{-1} \rightarrow 0$) and $2C_1 + 2C_2$ in the limit of small deformation($\lambda^{-1} \rightarrow 1$). Typical stress−strain isotherms, using the Mooney and Rivlin represention, are shown in Figure 1. Least-squares analysis was used to locate the best lines through these isotherms. The values of the constants $2C_1$ and $2C_2$ characterizing each isotherm are given in Table 2. According to some theories of rubber-like elasticity,[26,27] the ratio $2C_2/2C_1$ is a measure of the extent to which the elastic deformation changes from affine to nonaffine, characteristic of a *"phantom"* network, with increasing stress.

As can be seen from Table 2, for the networks *without free chains*, the modulus $2C_1 + 2C_2$ increases with decreasing the molecular weight between cross-links as expected.[28,29] However, the slope $2C_2$, which weighs the softening induced by the elongation, remains constant except for the intermediate molecular weight (M_{WH} = 10 200). On the contrary, a linear increase of the constant $2C_1$ with the cross-linking density is observed.

The values of $2C_1$ can be more qualitatively interpreted in terms of the "front factor" relating the elasticity constants to the average molecular weight of the networks chains. Specifically, the values of $2C_1$ listed in the table were interpreted with the use of the equation.[20,27]

$$2C_1 = C_3\, \rho k_B T/M_c \tag{3}$$

in which ρ is the density of the network and k_BT is the product of the Boltzmann constant by the absolute temperature, 298 K. The average molecular weight M_c between cross-links in the network is taken equal to M_n, the number average for the H−PS precursors, assuming completeness of the end-linking reaction. According to the theory for phantom networks,[30,31] the structure factor C_3 is predicted to be equal to $(1 - 2/f)$ where f is the network functionality, and should have the value of $^1/_3$ for a trifunctional network. As shown in Figure 2, this value is in good agreement with the experimental value $C_3 = 0.34$ for the networks without free chains RBHi (i = 1, 2, 3).

The values of $2C_2$, following classical rubber elasticity, can be interpreted in terms of the ratio $2C_2/2C_1$. This ratio would decrease when cross-links are more firmly embedded or constrained within the network structure. In practice, the experimental values of $2C_2/2C_1$, shown in Table 2, do indeed decrease down to very small values at low values of M_n. It is also of interest to note that the zero deformation modulus $2C_1 + 2C_2$ remains significantly lower than the corresponding value for a polystyrene melt (not cross-linked). Finally, the maximum elongation ratio before breaking, λ_{break}, increases with an increase in M_n (i.e., when the modulus $2C_1$ decreases).

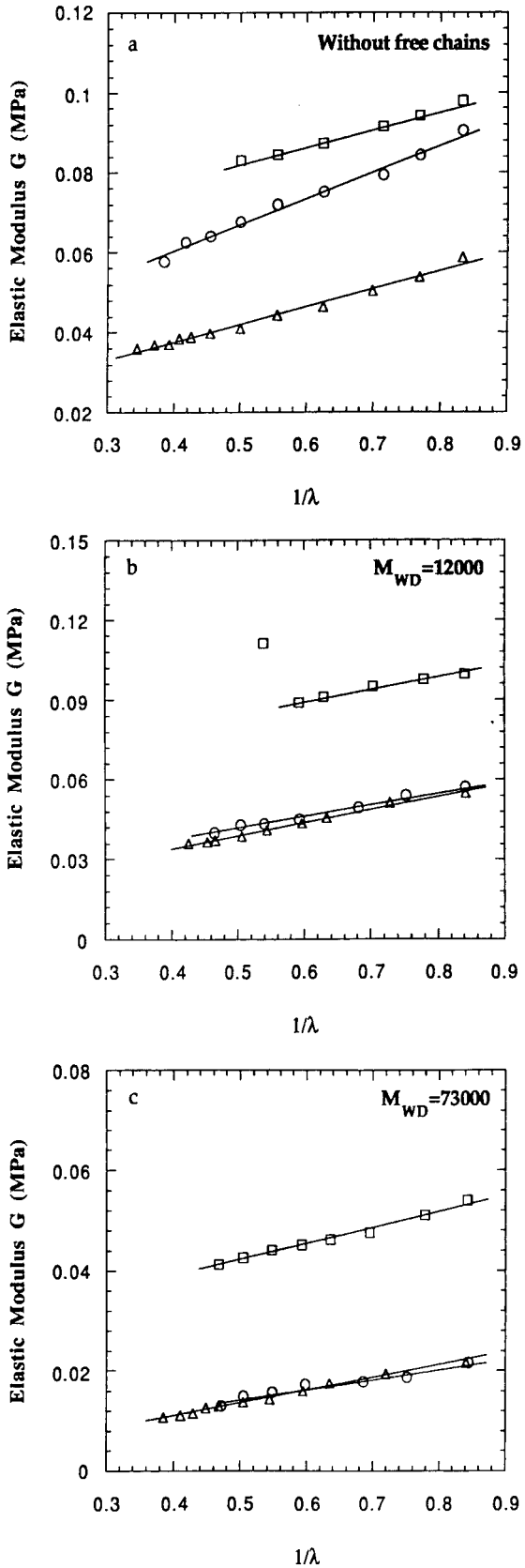

Figure 1. Mooney−Rivlin representation of the apparent modulus, G, against the inverse of the elongation ratio, $1/\lambda$: (a) samples without free chains; (b) samples with free chains of low molecular weight M_{WD} = 12 000; (c) samples with free chains of high molecular weight M_{WD} = 73 000.

Let us look now at networks containing *free chains with low molecular weight* (M_{WD} = 12 000). The slope

Table 2. Stress−Strain Results of the End-Linked Polystyrene Networks and Values of the Mooney-Rivlin constants $2C_1$, $2C_2$, $2C_1 + 2C_2$, and $2C_2/2C_1$ Obtained from Eq 2

sample	λ_{break}[a]	$2C_1$ (MPa)	$2C_2$ (MPa)	$2C_1 + 2C_2$ (MPa)	$2C_2/2C_1$	σ_0[b] (MPa)	G_0[c] (MPa)	G_{break}[d] (MPa)
RBH1	2	0.060	0.045	0.105	0.75	0.0130	0.080	0.083
RBH2	2.6	0.034	0.066	0.100	1.94	0.0260	0.059	0.059
RBH3	2.9	0.020	0.045	0.065	2.25	0.0220	0.034	0.035
RBH11	1.86	0.064	0.043	0.107	0.67	0.0103	0.085	0.087
RBH12	2.15	0.020	0.045	0.065	2.25	0.0150	0.037	0.041
RBH13	2.35	0.015	0.048	0.063	3.20	0.0200	0.033	0.035
RBH21	2.15	0.026	0.032	0.058	1.23	0.0110	0.039	0.041
RBH22	2.15	0.004	0.020	0.024	5.00	0.0080	0.012	0.013
RBH23	2.6	0.001	0.025	0.026	25.0	0.0130	0.009	0.011

[a] Elongation ratio at rupture. [b] True stress σ_0 at $\lambda \rightarrow 1$ limit. [c] Slope of the variation of σ against $(\lambda^2 - 1/\lambda)$. [d] Modulus before the rupture.

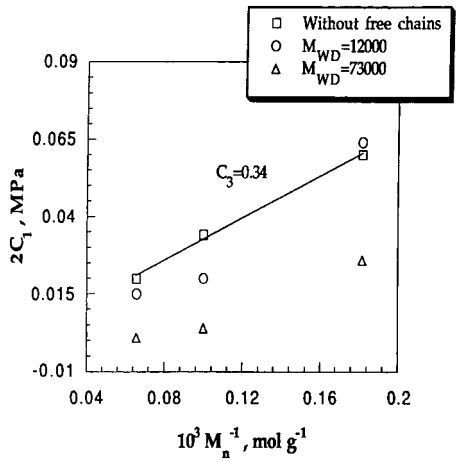

Figure 2. Elastic modulus, as represented by the constant $2C_1$, shown as a function of the reciprocal of the molecular weight of the network chains M_n. The straight line shows the least-squares fit of the experimental points for the networks without free chains to eq 3, yielding a slope $C_3 = 0.34$.

$2C_2$ is constant and close to the values without free chains. Similarly, the values of the modulus $2C_1$ (and therefore of $2C_1 + 2C_2$) do not vary strongly when the free chains are added. Going into more detail, one can point out three interesting features:

(i) The presence of free chains, even short, (RBH12, $M_{WH} = 10\,200$) reduces however systematically the values of the modulus G. Its variation with λ becomes close to that of sample RBH13 with $M_{WH} = 15\,500$.

(ii) For the sample with high cross-link density (RBH11, $M_{WH} = 5720$), a strong upturn in the modulus G is observed at the higher elongation due to the limited extensibility of the short network chains. Such a *hardening* effect has been observed by Tang and Mark for an end-linked bimodal network in which very short chains were mixed with a relatively long chains.[32]

(iii) The elongation ratios λ_{break} at which the samples broke (maximum extensibility) are somewhat lower than the values for the networks without free chains.

Finally, for the networks containing *long free chains* (RBH2i, $i = 1, 2, 3$; $M_{WD} = 73\,000$), a strong breakdown in the modulus G is observed. This is mainly due to the values of the elastic constant $2C_1$ which are extremely low, in particular for the samples with high molecular weight between cross-links (10 200 and 15 500, RBH22 and RBH23). One can attribute these low moduli to a strong disorganization of the cross-linking in presence of long chains. However, the values of the swelling ratio at equilibrium, another quantity widely used for characterizing the networks, remains surprisingly independent of the presence of free chains: as pointed out above, for each given M_{WH}, the values without or with chains either short or long are equal within the uncertainty of measurements. For all samples, the measurements of the swelling implies that the free chains would be washed out of the sample. Therefore, an equilibrium swelling indicates similar elasticities of the networks. The classical theory of elasticity does not predict any difference of behavior between the extensional modulus and the shear modulus which controls the swelling. It is quite striking that only the presence of chains inside the networks modifies the response to the deformation so much. At this stage, we can only acknowledge this difference.

Recently, some authors showed that another representation, σ vs $(\lambda^2 - \lambda^{-1})$, suggests that the tensile stress is the sum of two contributions:[33−35]

$$\sigma = \sigma_0 + G_0(\lambda^2 - \lambda^{-1}) \qquad (4)$$

σ_0 depends only on the chemical nature of the polymer and not on the cross-linking density while G_0 depends strongly on the cross-linking density.

For our data (Figure 3), this representation gives a linear variation within a certain range of deformation. The values of σ_0 and G_0 are listed in Table 2. The best range for the fit is difficult to define. Its lower band is affected by the deviation from the linear range: one must have $\sigma(\lambda \rightarrow 1) = 0$, but also the perfect definition of the initial length of the sample is difficult to achieve. The choice of the range has a strong influence on the value obtained for σ_0. Within this uncertainty, the values of σ_0 remain constant, and G_0 varies in a sensible way with the cross-linking ratio.

It is important to note that, at low deformations, a small deviation from the linear behavior is observed. Such an effect is normal ($\sigma(\lambda \rightarrow 1) = 0$) but could be enhanced by the adjustment of the initial length of the sample before deformation. The force after the first deformation can therefore be underestimated. As seen in Figure 3 for all our data, the values of σ_0 are approximately constant, with a considerable error because their determination is very sensitive to the range of λ chosen for the linear fit.

In summary, our mechanical measurements give sensible values of the usual parameters with respect to cross-linking ratio, in the absence of free chains. The presence of short chains does not affect strongly these values, whereas large chains seem to disorganize noticeably the network.

3.2. SANS Measurements: Isotropic State. 3.2.1. Effect of the Precursor Length. We consider first the scattering intensities of the samples containing free chains with high molecular weight ($M_{WD} = 73\,000$) measured in the isotropic state. Figure 4 shows their

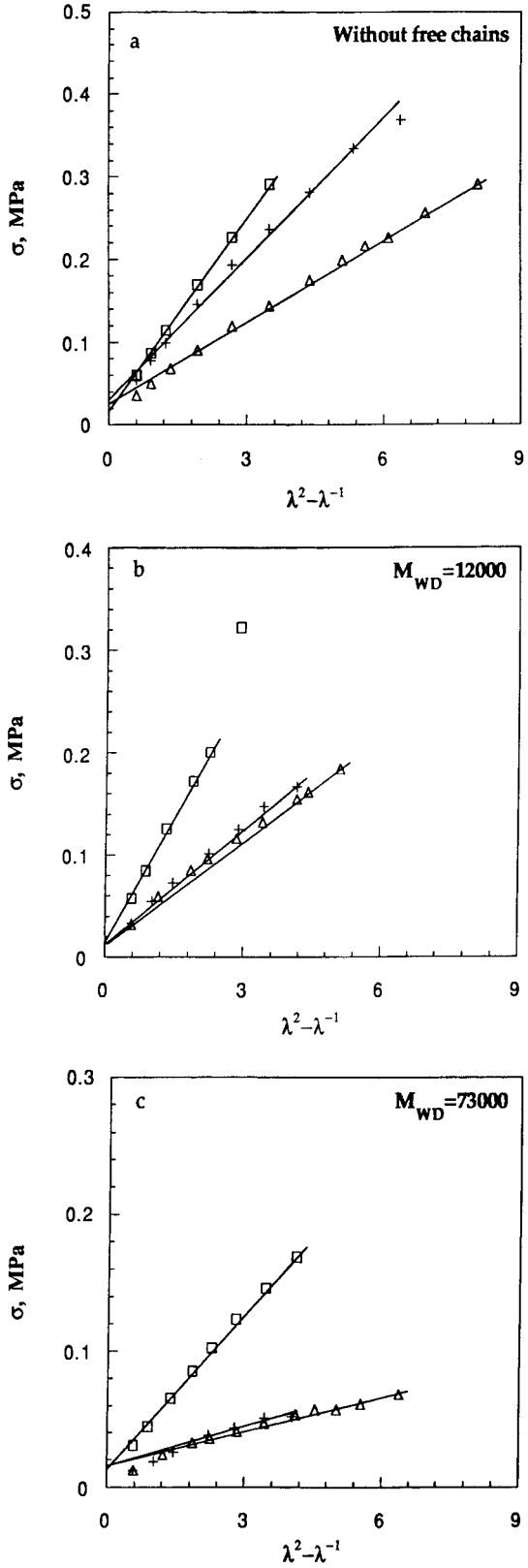

Figure 3. True stress, σ, as a function of $\lambda^2 - 1/\lambda$: (a) samples without free chains; (b) $M_{WD} = 12\,000$; (c) $M_{WD} = 73\,000$.

variations in a logarithmic representation. One can distinguish two different regimes:

(i) At low q, the scattering intensity increases continuously with increasing the cross-linking density (i.e., decreasing the molecular weight M_{WH} between cross-links). Furthermore, a large enhancement in intensity is observed for the network which is the most cross-linked ($M_{WH} = 5720$) while for the two other samples

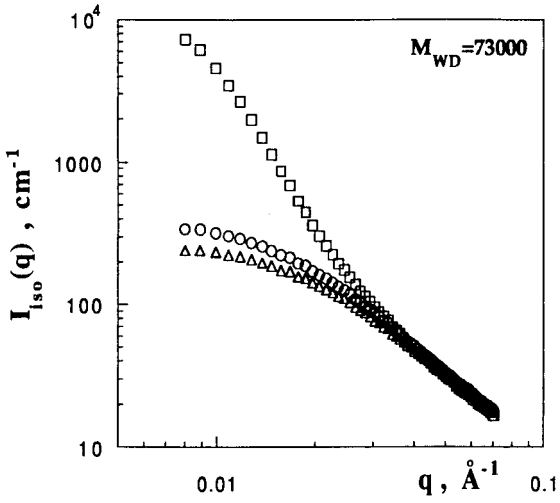

Figure 4. Logarithmic representation of the isotropic scattering for the samples with different cross-link density containing large free chains ($M_{WD} = 73\,000$): (□) RBH21; (○) RBH22; (△) RBH23.

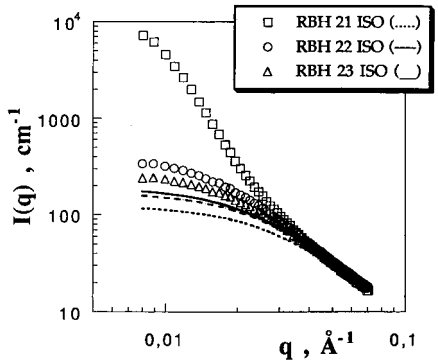

Figure 5. Comparison, in log−log representation, between the isotropic scattering from the samples with different cross-link density containing large free chains ($M_{WD} = 73\,000$) and the computed signal of an ideal mixture (melt). The calculated signals (···, - -, —) correspond to the samples RBH21, RBH22, and RBH23, respectively.

($M_{WH} = 10\,200$ and $15\,500$), the signals are not strongly different.

(ii) At high q values, all curves are quasi-identical; thus, the scattering does not depend upon the cross-linking density. One observes a $1/q^2$ variation, which leads to a plateau in the Kratky−Porod representation ($q^2I(q)$ vs q). We observe in this q range the form factor of a Gaussian chain.

Another way to determine the effect of the cross-linking is to compare our measurements to the signal obtained from the same deuterated chains randomly dispersed in a melt of the same chains as the one used for precursors for the network, but *without cross-linking*. In the absence of data, we have calculated the scattering for such an ideal mixture using the random phase approximation (RPA);[36] one sees in Figure 5 that it is much lower than that measured for the cross-linked samples. Similar effects have also been observed for randomly cross-linked networks.[1]

Qualitative Analysis: Debye−Bueche Law. We now focus on the sample of high cross-linking ratio ($M_{WH} = 5720$). The scattering is the signature of strong demixing characterised by the well-known Porod's law, which leads to a plateau in the $q^4I(q)$ vs q representation (Figure 6). An inhomogeneous biphasic system, with neat interfaces, yields such behavior.[37] Assuming a random distribution of the two phases at any scale,

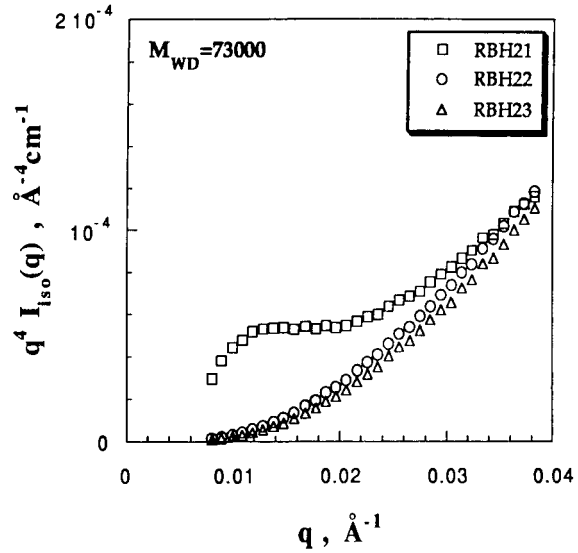

Figure 6. Porod representation, $q^4I(q)$ vs q^2, of the isotropic scattering for the samples with different cross-link density containing large free chains (M_{WD} = 73 000): (□) RBH21; (○) RBH22; (△) RBH23.

following Debye and co-workers,[38] the scattering intensity is given by the Debye−Bueche law

$$I(q) = I(q \rightarrow 0)/(1 + q^2\Xi^2)^2 \tag{5}$$

with

$$I(q \rightarrow 0) = 8\pi K_{eff}{}^2\Xi^3\phi(1 - \phi) \tag{6}$$

The size of the domains can be determined from the correlation length Ξ of the signal. In our case, we expect to have two phases of volume fractions ϕ and $(1 - \phi)$. One phase is rich in deuterated polystyrene PSD, but may contain a certain proportion of normal polystyrene PSH; the other phase is rich in PSH, but may contain a certain proportion of PSD. The effective contrast between the two phases is given by the relation

$$K_{eff}{}^2 = K_{max}{}^2(\phi_1 - \phi_2)^2 \tag{7}$$

where $K_{max}{}^2 = (a_H/v_H - a_D/v_D)^2$ is the real contrast of the mixture PSH/PSD. ϕ_1 and ϕ_2 represent the volume fraction of PSD in phases 1 and 2 respectively, and a_H and v_H (a_D and v_D) are the scattering length density and the partial volume of PSH (PSD).

For lengths above Ξ ($q\Xi < 1$), the scattering intensity $I(q)$ given by eq 5 varies slowly with q, similar to that of a form factor in the Guinier regime. A linear fit of the square root of inverse intensity (in absolute units), $1/I^{1/2}$ vs q^2, yields Ξ = 187 Å and $I(q \rightarrow 0)$. From eq 6, $K_{eff}{}^2$ is found to be five times lower than the maximum contrast $K_{max}{}^2$ expected for complete PSH/PSD demixing ($K_{max}{}^2/K_{eff}{}^2 \sim 5$). One can imagine two situations:

(i) A certain fraction of free chains are demixed in some regions in the network inducing a microphase separation while the other quantity remains distributed homogeneously in the network. This would lead to the scattering of a normal mixture $I_{mix}(q)$ superposed on a Debye−Bueche law.

(ii) Second, a strong expulsion of free chains occurred, leading to two phases or probably to a series of phases in the network with concentrations ϕ_{Di}. Note that this should give, at q large enough, a global scattering intensity which is the sum of the mixture signals in different phases $I_{mix}(q) = \sum_i \phi_{Di}(1 - \phi_{Di})/q^2$. In practice, we observe a $1/q^2$ law at large q, as predicted both by (i) and (ii).

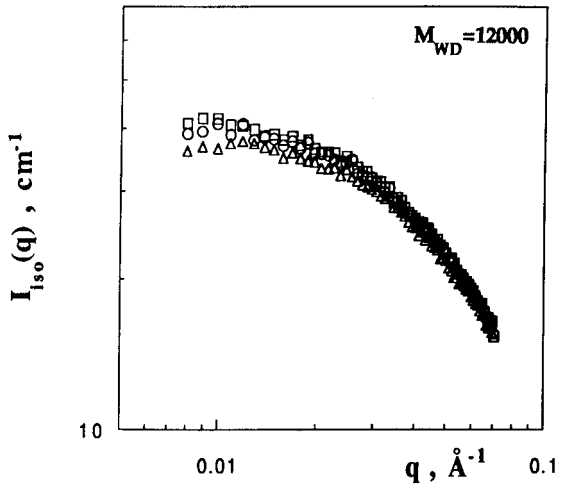

Figure 7. The log−log representation of the isotropic scattering for the samples with different cross-link density containing short free chains (M_{WD} = 12 000): (□) RBH11; (○) RBH12; (△) RBH13.

At intermediate q, as noted earlier, the data show a plateau in $q^4I(q)$ representation. The value of the plateau is proportional to $3/\Xi$. Knowing $K_{eff}{}^2$, we find Ξ = 283 Å, a value slightly different from that for the low q extrapolation (187 Å). This indicates that the system is slightly different from a simple biphasic random medium.

3.2.2. Effect of the Molecular Weight of the Free Chains. We now compare the series described above to another series of networks with the same precursors but with a lowest molecular weight of free chains (M_{WD} = 12 000). The scattering of an ideal mixture is therefore lower than the measured signal but the values of both signals are very close. One observes only (Figure 7) a weak increase in the scattering intensity with increasing cross-link density. Even for the largest density, no microphase separation occurs for the more cross-linked network with above values of M_{WD}.

3.3. Anisotropic State. 3.3.1. Effect of the Elongation: a Representative Example. Let us now consider the network with an intermediate cross-link density (M_{WH} = 10 200) containing free deuterated chains of the largest molecular weight, M_{WD} = 73 000. The sample is stretched uniaxially by a factor λ at high temperature (134 °C) and subsequently relaxed for a long time (t_R = 10 min). The elongation ratios λ were increased successively from 1 until the sample broke. $I_{\parallel}(q)$ and $I_{\perp}(q)$ are the radial average intensities within angular sectors parallel and perpendicular to the stretching axis, respectively. Figure 8 shows their variation with q. One observes an intensity similar to that observed earlier[1] for the statistical networks with the same molecular weight of the free chains. In the parallel direction, the scattering intensity $I_{\parallel}(q)$ increases progressively with λ at low q. In the perpendicular direction, $I_{\perp}(q)$ decreases slightly below the isotropic signal for λ = 1.2, and soon stabilizes close to the scattering of an ideal mixture for $\lambda > 1.2$.

A logarithmic representation makes a clear distinction between two q ranges for the variation of $I_{\parallel}(q)$: a plateau at low q and then a linear decrease at larger q. Increasing λ, the low q plateau increases in height and the crossover value $1/\xi_{\parallel}$ decreases progressively toward

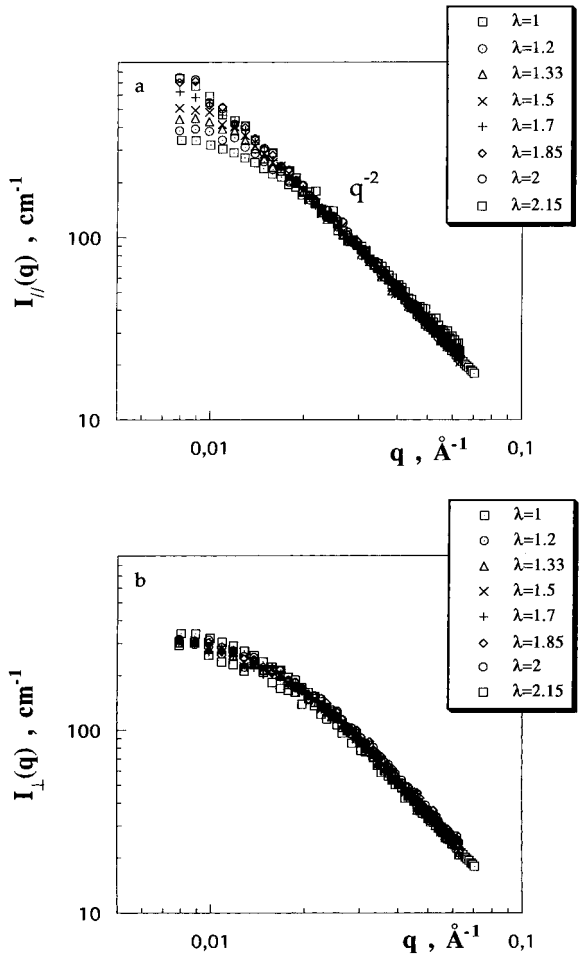

Figure 8. Scattering intensity, in log−log representation, in the parallel (a) and the perpendicular (b) directions for the sample RBH22, with an intermediate cross-link density and M_{WD} = 73 000, as a function of the elongation ratio λ.

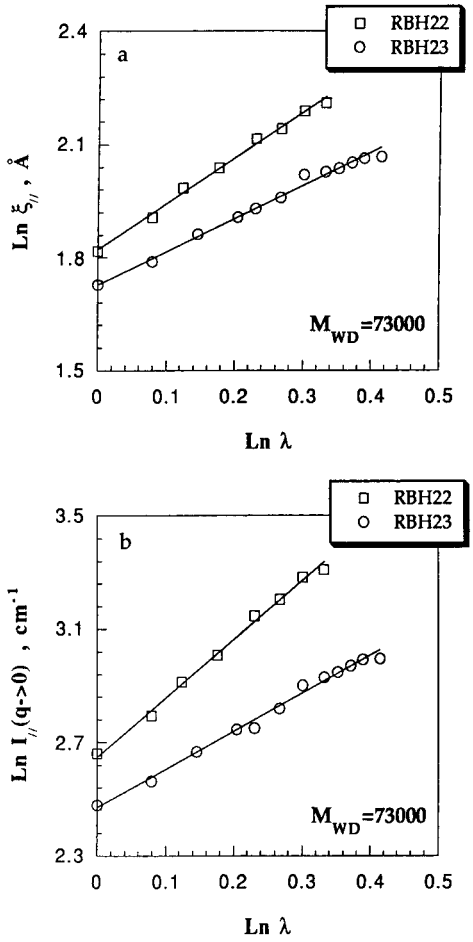

Figure 9. Variation of the correlation length $\xi_{||}$ (a) and the scattering at q-zero limit, $I_{||}(q \rightarrow 0)$ (b), in the parallel direction against the elongation ratio λ for the samples: (□) RBH22; (○) RBH23, containing large free chains (M_{WD} = 73 000).

lower q's. (i.e. the apparent correlation length increases). In $q > 1/\xi_{||}$, which is what could be called an intermediary regime, the curves are quasi-identical for all values of λ and collapse progressively to a *limit curve*. Finally, in a large q regime, the intensity remains similar to that for the isotropic case, i.e., to that for an ideal mixture.

The low q variation can be fitted to an Ornstein−Zernicke function

$$I_{||}(q) = I_{||}(q \rightarrow 0)/(1 + q^2\xi_{||}^2) \qquad (8)$$

Thus, as presented in Figure 9, the variations of $\xi_{||}$ and $I_{||}(q \rightarrow 0)$ with λ are close to power laws, with exponents close to 1.2 and 2, respectively. These exponents are lower than those for statistical networks (see Table 3). Altogether, the stretching effects are smoother here; this is also the case for the "limit curve", which is not as steep as for statistical networks (which is displayed as a power law $q^{-\alpha}$, $\alpha > 2$ for the same mass of the free chains). Finally, it is important to note the *absence of any change of behavior when approaching the rupture of the network*.

Analysis of the Dependence on the Angle ψ: Magic Angle. Instead of restricting ourselves to values of the angle between **q** and the stretching $\psi = 0°$ and 90°, corresponding to the parallel and perpendicular directions of q with respect to the stretching axis, we have explored all values of ψ within this range.

An initial method is to look at the isointensity lines on the detector (the curves joining the cells having recorded the same number of neutrons). They display the striking butterfly patterns (Figure 10), in the low q range.

Table 3. Values of the Apparent Exponents for the Power Law Variation of Correlation Length $\xi_{||}$ and the Scattering Intensity $I_{||}(q \rightarrow 0)$ with the Elongation Ratio λ

sample	$\xi_{||}$	$I_{||}(q \rightarrow 0)$
RBH11	0.60	0.64
RBH12	0.77	0.61
RBH13	0.77	0.40
RBH22	1.20	2
RBH23	0.86	1.33

A second procedure is to make a radial averaging within a series of ψ for a given elongation ratio. We then observe two interesting behaviors, similar to those of statistical networks: Figure 11 shows the variation of the scattering intensity $I(q,\psi)$ in a logarithmic representation for $\lambda = 2$, which is similar to the variation of $I(q)$ with λ at $\psi = 0°$ (i.e., to the scattering in the parallel direction). Furthermore, the signals $I(q,\psi)$ collapse on the *same limit curve*. Therefore, in a first approximation, the response of the scattering $I(q)$ is similar for all ψ, as long as the sample is dilated along the direction ψ.

One can actually calculate the dilatation along ψ; we know that when the sample is stretched by λ, it will be contracted in the transverse direction by a factor $1/\lambda^{1/2}$. The macroscopic extension ratio of the sample along the direction ψ, assuming an affine displacement of the mean positions of the junctions, is given by the relation

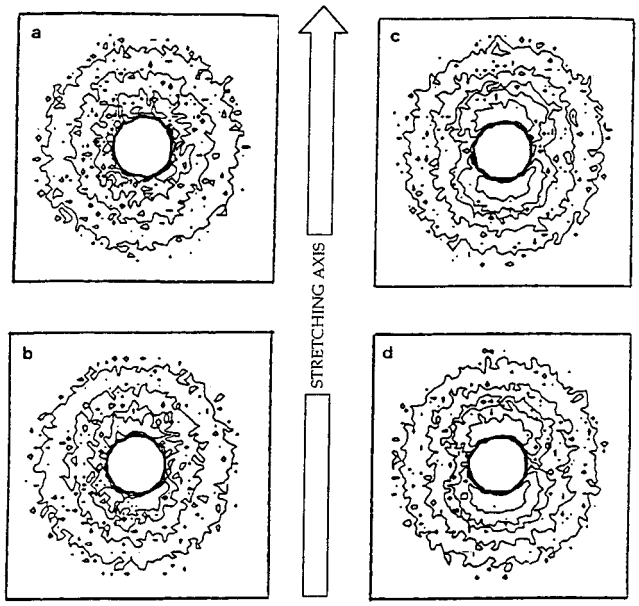

Figure 10. Isointensity patterns for the sample RBH22 for different values of the elongation ratio: (a) $\lambda = 1$; (b) $\lambda = 1.2$; (c) $\lambda = 1.85$; (d) $\lambda = 2$. The momentum transfer q is in the range: $7 \times 10^{-3} < q < 7 \times 10^{-2}$ (Å^{-1}).

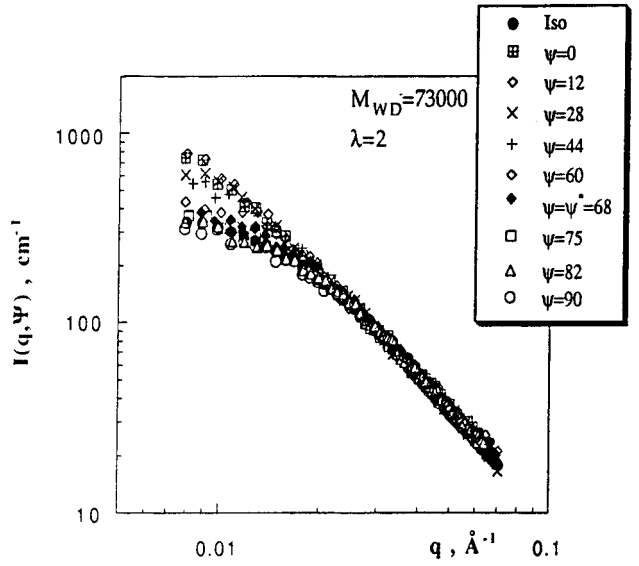

Figure 11. Scattering, in a log−log representation, for the sample RBH22 at $\lambda = 2$, for different angles between the parallel ($\psi = 0°$) and perpendicular directions ($\psi = 90°$). The value ψ^* corresponds to $\lambda^2 \cos^2 \psi^* + 1/\lambda \sin^2 \psi^* = 1$.

$$\lambda_{\text{eff}}(\psi) = (\lambda^2 \cos^2\psi + \sin^2 \psi/\lambda)^{1/2} \qquad (9)$$

which is valid for both junction affine and phantom network models.

One can extract the so-called "*magic angle*" ψ^* for which $\lambda_{\text{eff}}(\psi^*) = 1$. For a deformation $\lambda = 2$, we find $\psi^* = 68°$. We could expect to find $I(q,\psi^*) = I_{\text{iso}}(q)$ but do not. However, at this angle, an unexpected excess of the scattering is observed at values of $\psi \geq 75°$ which gives $I(q,\psi) < I_{\text{iso}}(q)$. This effect could be reduced if one rebins the data radially using a narrow angular sector.

3.3.2. Networks without Demixing. Long Free Chains. The effect of stretching, described above for the sample RBH22, is relatively similar to that for the other sample (RBH23) containing free chains of the same mass ($M_{\text{WD}} = 73\,000$). The sample corresponds to a lower cross-linking density ($M_{\text{WH}} = 15\,500$; the case of $M_{\text{WH}} = 5720$—biphasic—will be discussed below). The crossover values of q below which $I_{||}(q)$ increases with λ are comparable for both samples. $I_{||}(q)$ again progressively reaches a limit curve with a slope close to 1.75. These variations are observed here on a larger range of λ, since the sample broke later ($\lambda_{\text{break}} = 2.6$), as is often observed for weaker cross-linking. One has similar apparent exponents for the power law variations of $\xi_{||}$ and $I_{||}(q \rightarrow 0)$ with λ (Figure 9). The values extracted from the data are reported in Table 3.

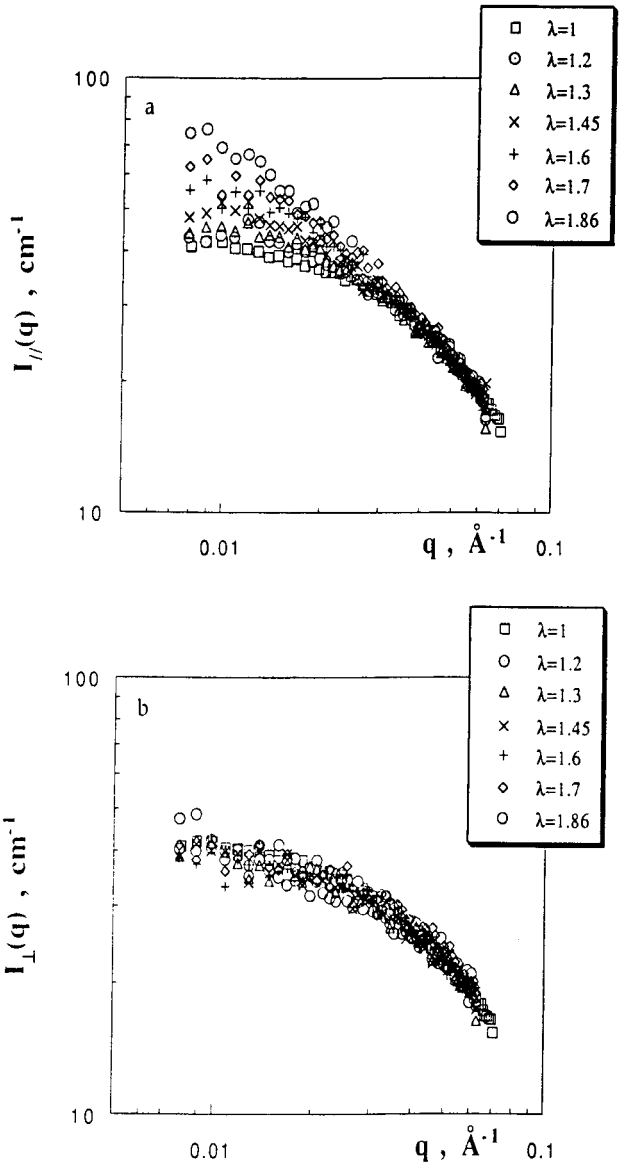

Figure 12. Scattering intensity, in log−log representation, in the parallel (a) and the perpendicular (b) directions for the sample RBH13, with low cross-link density and $M_{\text{WD}} = 12\,000$, as a function of the elongation ratio λ.

Short Free Chains. For short chains ($M_{\text{WD}} = 12\,000$), all signals are lower but respond to stretching similarly as above (see Figure 12 for sample RBH13 with low cross-link density). We note a few differences:

(i) Opposite to previous samples, it is difficult to define a limit curve.

(ii) The variations $\xi_{||}(\lambda)$and $I_{||}(q \rightarrow 0, \lambda)$, presented in Figure 13, are characterized by lower exponents of λ (Table 3).

(iii) For large λ, an upturn of $I_{\perp}(q)$ at very low q is observed in one case ($M_{\text{WH}} = 15\,500$).

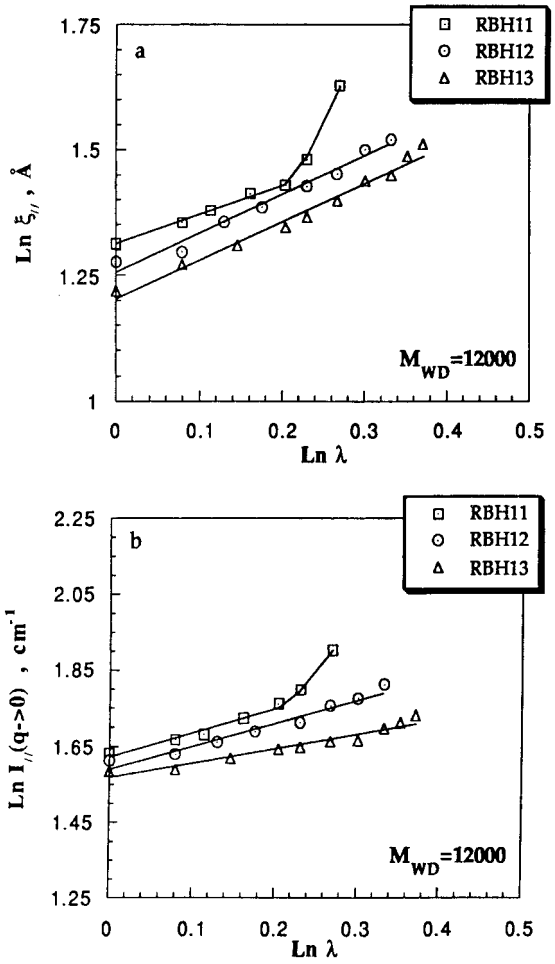

Figure 13. Variation of the correlation length $\xi_{||}$ (a) and the scattering at q-zero limit, $I_{||}(q \rightarrow 0)$ (b) extracted from eq 8, in the parallel direction against the elongation ratio λ for the samples: (□) RBH11; (○) RBH12; (△) RBH13, containing short free chains (M_{WD} = 12 000).

(iv) We observe the effect of a stronger cross-linking without demixing; *it shows an effect of the approach to breaking*: an additional increase in $\xi_{||}(\lambda)$and $I_{||}(q \rightarrow 0, \lambda)$ is observed; this could be associated with the additional increase of the modulus under the same conditions.

3.3.3. A Particular Case: Demixing Induced by Cross-Linking. As described above, the signal in the isotropic state of the most cross-linked sample (M_{WH} = 5720) containing free chains of high molecular weight M_{WD} = 73 000 (RBH21) is characteristic of demixing.

After the sample is stretched, $I_{||}(q)$ here *decreases with* λ: first strongly when λ increases from 1 to 1.2 and then more gently for higher λ, until the sample breaks (Figure 14). The apparent slope of the log−log plot decreases monotonically. In the perpendicular direction, one observes a smooth decrease of the intensity at low q and a smooth increase at intermediate q. As a consequence, the isointensity patterns reach a diamond shape[6] with a long axis perpendicular to the stretching direction (Figure 15). The butterfly patterns disappear.

This behavior is not easy to explain. We present only rather technical and incomplete remarks. First, the classical patterns corresponding to a long axis in the transverse direction are related to a deformation being affine, from large scales down to a low scale threshold. The scattering would then increase in the perpendicular and decrease in the parallel directions, and remain constant at high q. One could imagine an affine

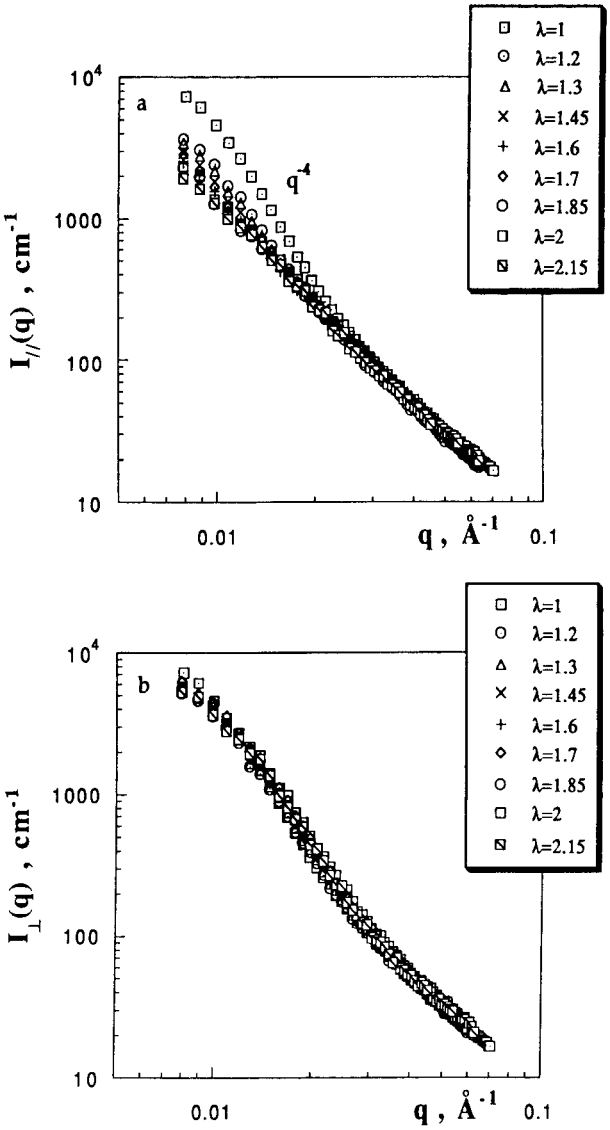

Figure 14. Scattering intensity, in log−log representation, in the parallel (a) and the perpendicular (b) directions for the sample RBH21, with high cross-link density and M_{WD} = 73 000, as a function of the elongation ratio λ.

deformation of the biphasic structure: the Porod's $1/q^4$ law would be shifted towards low q in the direction parallel to the stretching axis (by a factor logλ) and towards large q in perpendicular direction (by a factor of log$\lambda^{1/2}$).

Other processes are visible here. We only point out the following. (i) Some butterflies could arise from the inside of each phase. (ii) Butterfly patterns have also been observed for the scattering of biphasic media (where demixing is frozen by cross-linking). These additional processes could explain the observation by balancing the shifting of the region where Porod's law is obeyed. (iii) A network swollen by solvent absorbs more solvent under stretching. Similarly, phase demixing could be reversed back to a more homogeneous mixture; free chains could "remix" which would explain the disappearance of the Porod law behavior in the parallel direction but fails to explain the transverse behavior. Without being able to solve completely the problem, we finally point out that some values of $\Xi_{||}$ and $I_{||}(q \rightarrow 0)$ can be extracted from a linear fit of $1/I^{1/2}$ vs q^2. They follow the variation of $I_{||}(q)$: they decrease with λ ($\Xi_{||} \sim \lambda^{-0.64}$ and $I_{||}(q \rightarrow 0) \sim \lambda^{-2.1}$) as can be seen in

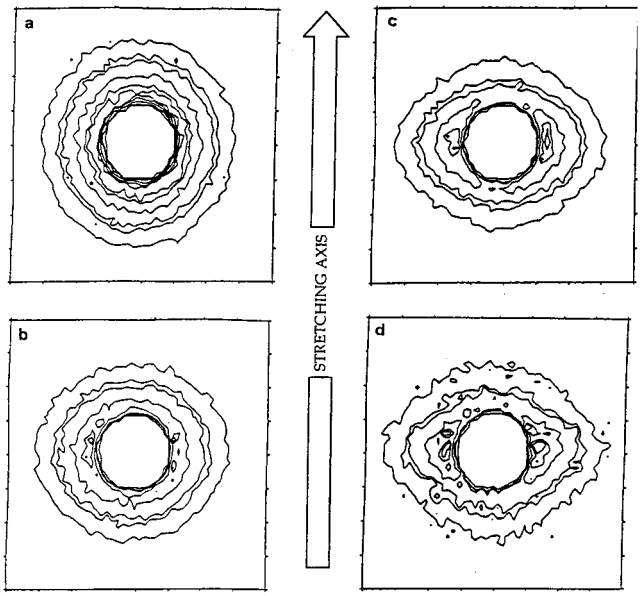

Figure 15. Isointensity patterns for the sample RBH21 for different values of the elongation ratio: (a) $\lambda = 1$; (b) $\lambda = 1.2$; (c) $\lambda = 1.7$; (d) $\lambda = 2.15$. The momentum transfer q is in the range: $7 \times 10^{-3} < q < 7 \times 10^{-2}$ (Å^{-1}).

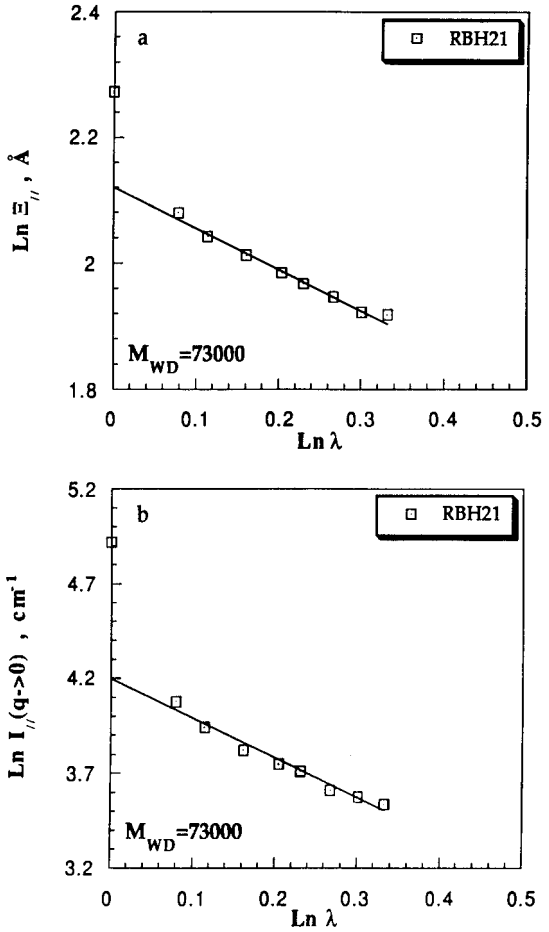

Figure 16. Variation of the correlation length $\Xi_{||}$ (a) and the scattering at q-zero limit, $I_{||}(q \rightarrow 0)$ (b) extracted from eq 5, in the parallel direction against the elongation ratio λ for the sample RBH21, containing large free chains ($M_{WD} = 73\,000$).

Figure 16. Their physical meaning remains to be established.

4. Discussion and Comparison with Theoretical Models. In this section, we shall first discuss the origin of butterfly patterns in polyurethane networks. We will compare the experimental results with recent theories which predict such an effect. These models are briefly described here. A more detailed description can be found in our recent paper.[1]

4.1. Spontaneous Fluctuations of Concentration Theory: Homogeneous Medium [Rabin−Bruinsma]. This phenomenological theory proposed by Rabin and Bruinsma[12] describes the physical properties of "soft" elastic solids constituting two components such as gels (swollen by a solvent), networks containing free species (chains, for example), or polymer melts (entangled chains). More precisely, this theory is derived for an *homogeneous system with spontaneous concentration fluctuations* of one of the components near the equilibrium state under *small* deformations.

In a simple theory, the volume fraction of the cross-linked polymer $\phi_0(\mathbf{r})$ is related to the displacement $\mathbf{u}$ under deformation by a conservation equation. Here additional fluctuations $\delta\phi$ are introduced, which remain coupled to the deformation via the term C_c div $\mathbf{u}$ $\delta\phi$ in the free energy. A minimization of the free energy leads to spontaneous enhancement of $\delta\phi$ along the parallel direction: if the concentration of free species is larger in some regions of the sample, these regions then become softer and therefore more elongated, and a new minimum is found for the total energy. One ends with the simple expression

$$S(q) \approx 1/(1 + q^2\xi_0^{\,2} - \Gamma(3\cos^2\psi - 1)) \qquad (10)$$

for a network swollen by solvent. Γ, proportional to $\lambda - 1$, is a dimensionless deformation. ξ_0 is the correlation length of the concentration fluctuations and ψ the angle between the stretching axis and the direction of observation.

Using the analogy with the "RPA" expression (eq 8),[36] one can rewrite eq 10, for a network permeated by free chains, as

$$S(q) \approx \{(1/\phi_H N_H + 1/\phi_D N_D)^{-1}(1/\phi_H N_H P_H(q) + 1/\phi_D N_D P_D(q)) - 2\chi_{HD} - \Gamma(3\cos^2\psi - 1)\}^{-1} \qquad (11)$$

where $P_H(q)$ and $P_D(q)$ represent the form factor of the network chains and the free chains respectively, and χ_{HD} is the Flory interaction parameter between the hydrogenated (H) and deuterated (D) chains.

The theoretical coherent scattering cross-section in absolute units (cm^{-1}) denoted $I_{cal}(q)$ is given by

$$I_{cal}(q) = (a_H/v_H - a_D/v_D)^2 v S(q) \qquad (12)$$

Along the parallel direction, the parameter Γ is positive and the scattering $S_{||}(q \rightarrow 0)$ increases with λ, while in the perpendicular direction, Γ is negative and $S_{\perp}(q \rightarrow 0)$ decreases.

Figure 17 shows a fit of eq 12 to some data for our representative sample ($M_{WH} = 10\,200$, $M_{WD} = 73\,000$). The front factor of $S(q)$ is adjusted at high q, where the intensity is less sensitive to the deformation. The values of $\Gamma_{||}$ are then obtained by adjustment at $q \rightarrow 0$. First, we see that for the isotropic state, where $\Gamma = 0$, eq 11 corresponds to a simple random mixing. The excess of the scattering could only be accounted for by additional terms as discussed in the next section. Second, under extension ($\lambda = 2$ in the figure), the fit is not satisfactory but a best value of $\Gamma_{||}$ can be obtained. The variation of $\Gamma_{||}$ with λ leads to new discrepancies. In theory, Γ should vary as $\lambda - 1$. In practice, such a

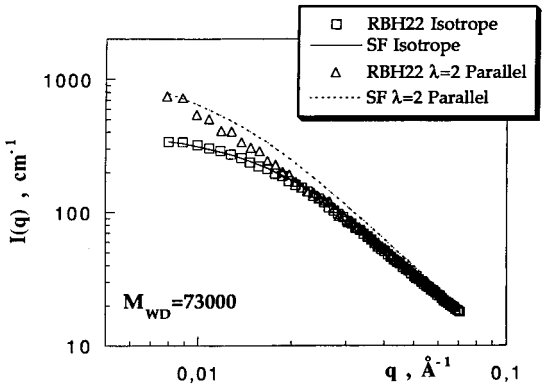

Figure 17. Comparison, in log−log representation, between the experimental scattering for the sample RBH22 and the spontaneous fluctuations model of Rabin and Bruinsma (SF) at $\lambda = 1$ (□, —) and $\lambda = 2$ (△, ···).

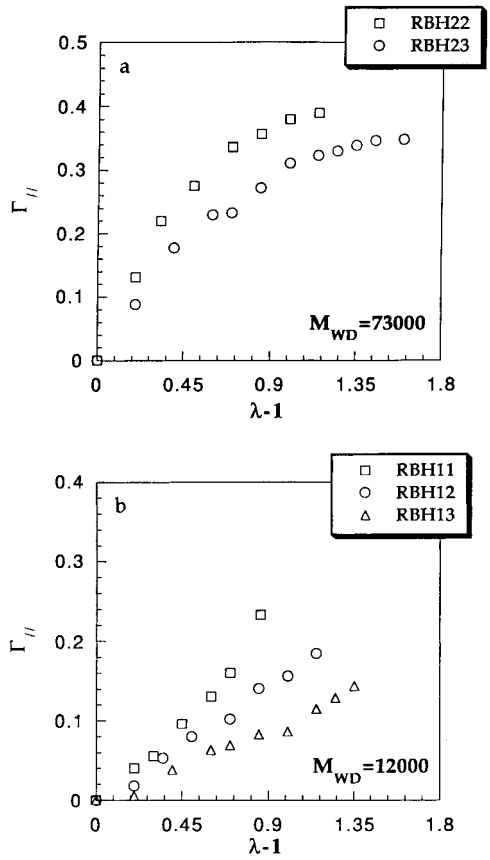

Figure 18. Variation of the dimensionless parameter $\Gamma_{||}$ against $\lambda - 1$, extracted by fitting the data to eq 11 in the parallel direction, for samples with $M_{WD} = 73\,000$ (a) and $M_{WD} = 12\,000$ (b).

linear variation is only obtained below $\lambda = 1.6$ (Figure 18). If the linearity was maintained at higher values, Γ would rapidly become larger than $\Gamma_s = 0.5$, the threshold for which $S(q)$ becomes infinite and decomposition should occur.

Since no decomposition is observed, Γ is bounded to values lower than 0.5. On the other hand, the data for short free chains are easier to fit since the variation of $I(q)$ with λ is much weaker. The fits of $I(q)$ are more satisfactory; Γ displays a linear variation with $\lambda - 1$, and remains below 0.5.

One can change the angular dependence of ψ in the expression of $S(q)$ using the term $(\lambda^2 \cos^2 \psi + \sin^2 \psi/\lambda - 1)$ instead of the expression $(\lambda - 1)(3 \cos^2 \psi - 1)$ which is valid only at low λ. This new term better describes the results at high λ, but a strong discrepancy is still observed in the variation of $\Gamma_{||}$, which becomes proportional to $(\lambda^2 - 1)$ instead of $(\lambda - 1)$ in the stretching direction.

In summary, this theory predicts butterfly patterns oriented in the same direction as that observed but does predicts neither the limit curve behavior, nor the soft power law variation of the correlation length ξ with λ which depends on the system. Moreover, at high deformation, this theory could not explain the saturation effect observed experimentally and the predicted isointensity lines should be modified by changing the ψ dependence in the scattering intensity $S(q)$.[1]

4.2. Enhancement of Thermal and Frozen Fluctuations [Onuki]. Another model based on the classical rubber theory proposed by Onuki[13] considers an *heterogeneous* network with a *frozen* cross-link density randomly distributed and assumed as a perturbation, $\nu = \nu_0 + \delta\nu$, where ν_0 is the average cross-link density and $\delta\nu$ is the deviation from this average value. The local concentration of the free species in the network is as usual controlled by the equilibrium between the elastic energy of deformation and the mixing entropy.

The total intensity is assumed to be the sum of two uncorrelated terms: the scattering from the *thermal* fluctuations $S_{th}(q)$ and that from the *frozen* density fluctuations $S_{fr}(q)$

$$S(q) = S_{th}(q) + S_{fr}(q) \tag{13}$$

In the case of a blend of free chains in a network, one can write the thermal term as

$$S_{th}(q) \approx 1/[(1/\phi_H N_H + 1/\phi_D N_D)^{-1}(1/\phi_H N_H P_H(q) + 1/\phi_D N_D P_D(q)) - 2\chi_{HD} + \mu^* J(\psi)] \tag{14}$$

similar to eq 10, but with an additional term. This term contains the dimensionless parameter $\mu^* = \mu v/k_B T$ where μ is the shear modulus and v is the specific volume of the monomer ($v \sim a^3$). It accounts for the effect of the cross-linking on the thermal fluctuations. This term is classical in a continuous theory of elasticity.[1,13,43−45]

On the other hand, the response of the system to frozen density fluctuations, under extension and swelling, leads to a quadratic term

$$S_{fr}(q) \approx p^{**}(\alpha^{-2} - J(\psi))^2 [S_{th}(q)]^2 \tag{15}$$

the ratio $\alpha = (\phi/\phi_0)^{-1/3}$ corresponds to swelling or deswelling with respect to the reference state (concentration ϕ_0), and $J(\psi)$ corresponds to stretching:

$$J(\psi) = \lambda^2 \cos^2 \psi + \sin^2 \psi/\lambda \tag{16}$$

p^{**} is a dimensionless number related to the degree of irregularity in the network structure and must be fitted to the data.

As above, we choose the sample RBH22 to test the validity of this theory. In eq 14, the term $\mu^* J(\psi)$ is positive, therefore *reducing* the scattering, as actually expected in classical theory of elasticity. In order to account for the *higher* scattering, we can only use the term χ_{HD}, which we need to take equal to 4×10^{-3}, i.e., 20 times the value for the blend h-PS/d-PS (2×10^{-4} at 134 °C). It is therefore obvious that it plays here an empirical role and that eq 14 is somehow incomplete. Let us anyhow introduce our best fit of S_{th} in eq 15 and

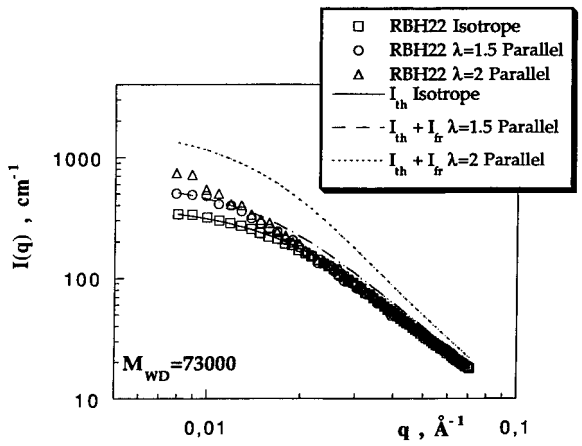

Figure 19. Comparison, in log−log representation, between the experimental scattering for the sample RBH22 at $\lambda = 1$ (□, —), $\lambda = 1.5$ (○, - -), and $\lambda = 2$ (△, ···) and the perturbation model of frozen fluctuations of cross-link density of Onuki, in parallel direction with the following parameters: $\alpha^{-2} = 1$, $\mu^* = 0$, $p^{**} = 4 \times 10^{-3}$ and $2\chi = 8 \times 10^{-3}$.

look at the data for $\lambda = 1.5$. Even in a more pronounced way than in the previous section, the fit over the intermediary range is very poor (Figure 19). It is because $S_{fr}(q)$ dominates the low q scattering, and varies as $1/q^4$ in the intermediary range. Only the experimental zero-q limit can be accounted for by using $p^{**}(\lambda = 1.5) = 4 \times 10^{-3}$. If we now consider the case $\lambda = 2$, this value of p^{**} leads to a strong overestimation of the data. Namely, the frozen contribution increases too strongly with λ.

The variation of the apparent correlation length, ξ_{th}, is on the contrary too weak compared to the data. The main reason is that the predicted scattering is soon dominated by the frozen contribution, which imposes a *constant* correlation length. Another discrepancy is about the direction perpendicular to stretching: if $\alpha = 1$, eq 15 should also lead to an increase, which is never observed in this direction. If α was taken lower than 1 ($\alpha < 1$), the term $(\alpha^{-2} - J(\psi))^2$ should first decrease and then rapidly increase: this is not observed.

Finally, we mention that the thermal term, if alone, would lead to butterflies with a great axis transverse to stretching ("*normal*" butterflies). This trend could appear in the theoretical form, for certain values of p^{**}, α, and λ, but has never been observed.

In summary, the model is not appropriate due mainly to the expression chosen for $S_{fr}(q)$ and its variation with q, with λ, and with ψ. These conclusions are, for this model as for the former one, qualitatively the same as those for statistical networks.[1]

4.3. "Cluster-Like" Heterogeneities Model: Geometrical Picture [Bastide et al.]. In this model, the butterfly patterns are attributed to the heterogeneities of structure which are assumed to preexist in the material. These fluctuations could be induced by the chemical cross-linking or by the entanglement of very long precursor chains. As a result, some more *cross-linked* or more *entangled* regions in the network can be represented as a kind of "superstructure", which contains less of the mobile species than average and vice versa.[10,11] These concentration fluctuations are frozen but are not treated as a perturbation contrary to the Onuki consideration.[13] This approach considers the situation where the large-scale concentration heterogeneities do not appear during the preparation of the network but become visible only under swelling by the mobile species, or by stretching.

This third model has been described in many papers, and the means by which one adapts it to the case of free chains permeating the network has also been described in detail recently.[1] It also considers frozen heterogeneities, but treats the response to stretching differently from Onuki because it assumes a different spatial distribution for the local cross-linking density. The model was developed for a semidilute solution of extremely large polymer chains cross-linked almost instantaneously in a random fashion. Before cross-linking, the solution can be visualized as a melt of "blobs" of size ξ_b, which scales as the screening length of the excluded volume interactions or as the distance between interchain contact points. The random and rapid cross-linking is described as a site percolation,[46] on a lattice with a site having the blob size. Thus, one forms an assembly of *polydisperse branched clusters* (frozen blobs). In a certain range of cross-linking density, the clusters are expected to spread over large length scales and to carry strong spatial correlations.

Under swelling or stretching, one can expect that the frozen blob clusters will swell or deform less than the average. They will be mostly displaced as a whole, inside a "sea" of less cross-linked material, undergoing most of the swelling or stretching. Because the clusters created by a percolation process are very much interpenetrated, they will disinterpenetrate along any direction of dilatation of the sample, and the correlation length will increase significantly. This is particularly important when the clusters are very polydisperse, as in the case of percolation. Then the small clusters will disinterpenetrate large clusters. An analogy can be drawn with the dilution of percolation clusters made by cross-linking of short polymer units, just below the gelation threshold. From Daoud and Leibler,[47] one has a new correlation length ξ_c

$$\xi_c \sim \phi^{-5/3} \tag{17}$$

$$S(q \to 0) \sim \phi \xi_c^{\,D} \sim \phi^{-5/3} \tag{18}$$

$$S(q) = S(q \to 0)/(q\xi_c)^D \tag{19}$$

$$\sim q^{-8/5} \qquad \text{for } q > 1/\xi_c$$

where ϕ is the polymer volume fraction and $D = D_f(3 - \tau)$ is the apparent fractal dimension which depends on the polydispersity of the clusters (described by τ) and on their fractal dimension, $D_f = 2$.[48] The same exponents were found for the scattering of a gel under swelling (ϕ still being the polymer fraction) in a particular case.[17] Lower exponents were found for some other gels.

In our case, the situation is a little bit different and the above model should not be directly applied. On the one hand, the networks are end-linked with a constant molecular weight between the junctions. We will discuss later the origin of the heterogeneities present in such networks. On the other hand, the networks are slightly swollen by the polymer chains (introduced during the preparation) and not by a good solvent. As mentioned elsewhere,[1] one can suggest two extreme possibilities: (i) the labeled chains are expelled from all clusters of different sizes, and then $S(q) \sim q^{-D_f(3-\tau)} \sim q^{-2}$ in the intermediate q range; (ii) the free chains are expelled only from the inside of the larger clusters, and then $S(q) \sim q^{-D_f} \sim q^{-2.5}$ (D_f is now the fractal dimension of one given large cluster, i.e., with no polydispersity).

Under stretching, a simple analogy between swelling and deformation leads to $\phi^{-1/3} \sim \lambda(\psi)$ (i.e., λ in the parallel and $1/\lambda^{1/2}$ in the perpendicular direction). Then, using eqs 17 and 18

$$\xi_{||} \sim \lambda^5 \qquad \xi_{\perp} \sim \lambda^{-5/2} \tag{20}$$

$$S_{||}(q \to 0) \sim \lambda^5 \qquad S_{\perp}(q \to 0) \sim \lambda^{-5/2} \tag{21}$$

These equations lead, at low q, to an increase of the scattering in the parallel direction and a decrease in the perpendicular and therefore to the observed butterflies. Moreover, eq 19 corresponds to the rise of a "limit curve" on a wider and wider q range, as ξ_c is progressively increasing. So the *qualitative* behavior is similar to what we observe. The behavior in the transverse direction requires however a closer look. From the experiment, we observe that $S_{\perp}(q)$ decreases only slightly at the beginning and then becomes quasi-independent of λ at low q. The detailed explanation could be as follows. In the isotropic state, the chains are partly or completely expelled from the soft regions. However, these regions are rather strongly interpenetrated and the difference from ideal mixing is relatively small. Under contraction in the transverse direction, only a limited interpenetration is possible when λ passes from 1 to 1.2−1.6. $S_{\perp}(q)$ decreases at this stage, and remains subsequently constant, since no important reinterpenetration is visible any more (in other words, the perpendicular correlation length becomes masked by the correlation length corresponding to ideal mixing, which is close to the radius of gyration of the chains).

However, there are quantitative discrepancies:

(i) Exponents in eqs 20 and 21 are higher than the observed one. This was already found for swollen gels under stretching.

(ii) The predicted limit curve should correspond to a power law. This is the case here only for $M_{WD} = 73\,000$. The exponent is $D_{app} = 2$. This could agree with the case of "polydisperse" clusters (see paragraph above) but is not a well-defined test of the model. For short free chains, neither the limit curve is reached nor is it a power law.

At this stage, we are tempted to propose that the limit curve will actually depend on the sample and characterize the "structure" of the network. This structure will also be only partly revealed for too short free chains at such small volume fractions.

In the above proposal, the contribution of the heterogeneities comes directly via a unique term, at variance with the Onuki model which contains an additional term. However, it was observed earlier, for some gels under swelling, that a term additional to the "thermal" one could allow good fits of the scattering, and a sensible variation of the parameters with cross-linking.[49] Recently, the same results for end-linked PDMS gels under swelling[50] have been found. Both Geissler et al.[49] and Rouf et al.[50] suggest the additivity by the shape of the curves: in a logarithmic representation, two successive plateaus were observed, both followed by a steep region. The scattering $I(q)$ seems to be dominated at low q by a "frozen" contribution and at large q by a "thermal" ("solution like") contribution.

In our present data for stretching, no such double plateau is seen. However, it remains possible that the "thermal" plateau is hidden by the low q contribution. Indeed, recent theoretical calculations made by Rabin and Panyukov show that this can be the case.[54] Their model contains the idea of frozen heterogeneities created by random cross-linking (other types of cross-linking are not excluded but have not been yet investigated). This idea is introduced into a more elaborate theoretical model, which assumes that the frozen contribution is additive. The final predictions agree qualitatively with a large set of data for gels, swollen or stretched.

4.4. What Could be the Origin of the Heterogeneities in the Polyurethane Networks? According to the above theories and most of the experimental results, the appearance of butterfly patterns in the randomly cross-linked networks is due essentially to the anisotropic unscreening of more cross-linked clusters. Then, one can raise the following questions: Are there also some forms of heterogeneities in polyurethane networks, since in such systems we observe the butterfly anomaly as well? What is the efficiency of the end-linking reaction? One important effect has already been discussed above: the value of the modulus (especially $2C_1$) is diminished by the presence of long chains. This could indicate an important disorganization of the cross-linking; however, we also remarked that the equilibrium swelling was not affected by free chains. Moreover, end-linked networks of the same chemistry, have been investigated (in absence of free chains) under swelling by a deuterated solvent. They also displayed an increase in the scattering with swelling,[16,17] as for statistical networks. Other origins of heterogeneous cross-linking were therefore proposed, which will we detail now.

The information is partly contradictory:

(i) The conversion rate of one tris(isocyanate) arm in the urethane connections (defined as the rate of the reacted arms in the tris(isocyanate) functions) is estimated from the infrared measurements to be 97%[16] or 98%,[17] while the rate of the chains extractable by solvent washing the networks is found to be close to 2%, which corresponds to a conversion rate of 86%.

(ii) The equilibrium swelling ratio Q_{eq} of the networks by toluene was found to be 12, 15, and 19 for the networks $M_{WH} = 5720$, 10 200, and 15 500, respectively, which are different from the values found for the same category of samples (without free chains) investigated in this paper ($Q_{eq} = 7.8$, 10.2, and 12).

(iii) The commercial tris(isocyanate) material contains noticeable quantities of tetrakis- and pentakis(isocyanate). This material was not purified before use. On the other hand, the end-linking reaction is very sensitive to H_2O. Even if the all materials and the reaction device were heated under vacuum and argon before use, a risk remains possible during the injection of the solution into the mold.[51]

Hence, one cannot strictly exclude the possibility that the functionality of some junctions is *two* instead of *three*. This produces a dangling chain and a larger chain between cross-links. The resulting networks could be closer to statistical samples.

It is important to note that even for a total conversion rate (100%), some heterogeneities could be created in the network.

(i) One reason is due to the random partition of the entanglements. Their arrangement is not necessarily regular, leading to an intrinsic disorder in the network. In analogy with the situation of the randomly cross-linked networks, one may anticipate the existence of more entangled clusters, eventually with a characteristic size larger than the average distance between entanglements.

(ii) A second reason is the irregular topology of the network. We have already stressed that the latter could be strongly different from the regular railing, mapped on the geometry of a crystalline lattice.[5,52] On the contrary, one could have much larger loops, even with perfectly trifunctional junctions. A similar picture was proposed recently[50] in order to interpret the scattering of swollen PDMS gels end-linked in the bulk. For these samples, the observation of static speckles using coherent light scattering shows that the static contribution is enhanced along the parallel direction.[53] Straube *et al.*[54] proposed a tube model, based on a self-consistent mean-field approach, for entanglement systems subjected to an uniaxial deformation. Assuming a nonaffine deformation, the model predicts for labeled chains cross-linked within a network isointensity contour lines with the same ellipsoidal−lozengic transition as observed experimentally. But it is important to notice that the model does not predict butterfly patterns for networks containing labeled free chains even larger than the network chains. This is also true for networks with high entanglement density.

In summary, the heterogeneities in the end-linked networks could be created by an imperfect cross-linking, by the presence of free chains, or by the arrangement of an irregular topology.

5. Summary and Conclusions

We have measured the scattering intensity from end-linked networks containing a small proportion of deuterated free chains under uniaxial deformation and compared the results to those obtained earlier from randomly cross-linked networks. The end-linked networks are made by linking protonated precursor chains by functional groups placed at their ends. Three molecular weights M_{WH} of the precursor chains have been used, 5720, 10 200, and 15 500, leading to three cross-link densities, while the molecular weights of the free chains M_{WD} are chosen to be equal to 12 000 and 73 000. The samples were stretched up to rupture. We have focused our interest on the phenomenon of "butterfly patterns" appearing in the isointensity lines. Different models have been discussed.

The model of spontaneous enhancement of fluctuations (thermal) under strain[12] gives the correct orientation of the butterfly patterns, and the correct dependence upon ψ after a little modification. But it fails to account for the q profile of $I(q)$ and fails at large deformation, predicting too large an effect.

The two other models consider frozen fluctuations. The perturbation model of Onuki[13] gives a "frozen" contribution which also varies too strongly with λ: it is impossible to fit data at different λ with the same parameters. It does not explain the stability of the transverse scattering. The possibility of various orientations of the axis of the butterfly patterns is nested in the expression of the thermal scattering, but this has not been observed until now.

The third model is the only one which could explain the progressive increase of $I_{\parallel}(q)$, together with stagnation of $I_{\perp}(q)$. It predicts the formation of regions of higher cross-linking density having the characteristics of percolation-like clusters.[10,11] It attributes the formation of the butterfly patterns to some anisotropic unscreening of clusters. The clusters would consist of branched or interpenetrated regions of higher rigidity, i.e., less deformed than some softer interstitial parts, in which the concentration of the labeled chains would be lower than average. This model predicts power law variations for the correlation length ξ and the zero-q intensity $I_{\parallel}(q \rightarrow 0)$ with λ but with exponents higher than the measured values. Thus, it remains qualitative.

Finally, more recent work,[55] assumes the additivity of thermal and frozen contributions. The frozen part could come from the randomness of the cross-linking or from some other structure specific to a given network. It seems that the order of magnitude of the variation of $I(q)$ as a function of swelling or of stretching ratio can be accounted with approximately constant parameters. These parameters have a physical meaning related to the description of a random cross-linking, but a more detailed fitting procedure should be undertaken.

Our conclusions are qualitatively the same as for statistical networks. It seems that spatial heterogeneities in the cross-linking density are also present for end-linked networks. It could be due to imperfect chemistry (too low or too high functionality of some junctions), which cannot be ruled out. But it could be also due to heterogeneous structures even after perfect end-linking: entanglement heterogeneities or the presence of large loops. We recall that some other end-linked networks (PDMS cross-linked in bulk) display similar effects (through the q profile, which becomes quite different for large precursors) after swelling and stretching.

Acknowledgment. We are grateful to M. Geoghegan for kindly reviewing the manuscript.

References and Notes

(1) (a) Ramzi, A.; Zielinski, F.; Bastide, J.; Boué, F. *Macromolecules* **1995**, 28, 3570−3587. (b) Ramzi, A. Thesis, Université Pierre et Marie Curie, Paris VI, Paris, France, 1994.
(2) (a) Zielinski, F.; Buzier, M.; Lartigue, C.; Bastide, J.; Boué, F. *Prog. Colloid Polym. Sci.* **1992**, 90, 115. (b) Zielinski, F. Thesis, Université Pierre et Marie Curie, Paris VI, Paris, France, 1991.
(3) (a) Oeser, R.; Picot, C.; Herz, J. In *Polymer Motion in Dense Systems*; Richter, D., Springer, T., Eds.; Springer Proceedings in Physics 29; Springer-Verlag: Berlin, 1988; p 104. (b) Oeser, R. Thesis, University of Mainz, Mainz, Germany, 1992.
(4) Boué, F.; Bastide, J.; Buzier, M.; Collette, C.; Lapp, A.; Herz, J. Proceedings of the Gomadingen Meeting of October 1986. *Prog. Colloid Polym. Sci.* **1987**, *75*, 152−170. Boué, F.; Bastide, J.; Buzier, M. *Molecular Basis of Polymer Networks*; Springer Proceedings in Physics; Springer: Jülich, Germany, 1988; Vol. 42, pp 65−81.
(5) Onuki, A. In *Space-Time Organization in Macromolecular Fluids*; Tanaka, F., Ohta, T., Doi, M., Eds.; Springer Proceedings in Physics; Springer: Berlin, 1989; p 94.
(6) Inoue, T.; Moritani, M.; Hashimoto, T.; Kaway, H. *Macromolecules* **1971**, *4*, 500.
(7) Wu, X. L., Pine, D. J., Dixon, P. K. *Phys. Rev. Lett.* **1991**, *66*, 2408.
(8) Hashimoto, T.; Kume, T. *J. Phys. Soc. Jpn.* **1992**, *61*, 1839.
(9) Boué, F.; Lindner, P. *Europhys. Lett.* **1994**, *25*, 421.
(10) Bastide, J.; Leibler, L. *Macromolecules* **1988**, *21*, 2647.
(11) Bastide, J.; Leibler, L.; Prost, J. *Macromolecules* **1990**, *23*, 1821.
(12) Rabin, Y.; Bruinsma, R. *Europhys. Lett.* **1992**, *20*, 79.
(13) Onuki, A. *J. Phys. II* **1992**, *2*, 45.
(14) Mendes, E.; Boué, F.; Bastide, J. To be published in *Macromolecules*.
(15) Richards, D. H.; Szwarc, M. *Trans. Faraday Soc.* **1959**, *55*, 164.
(16) Hakiki, A. Thesis, Université Louis Pasteur, Strasbourg, France, 1991.
(17) Mendes, E. Thesis, Université Louis Pasteur, Strasbourg, France, 1991.
(18) Gérard, E. G. Thesis, Université Louis Pasteur, Strasbourg, France, 1988.
(19) This time is fixed to 10 min and is much higher than the stretching time (estimated to be 10 s). The sample is assumed to be close to equilibrium under tension.

(20) Mark, J. E.; Sullivan, J. L. *J. Chem. Phys.* **1977**, *66*, 1006.
(21) Mark, J. E.; Flory, P. J. *J. Appl. Phys.* **1966**, *37*, 4635.
(22) Mark, J. E. *Rubber Chem. Technol.* **1975**, *48*, 495.
(23) Flory, P. J.; Tatara, Y. *J. Polym. Sci., Polym. Phys. Ed.* **1975**, *13*, 683.
(24) Treloar, L. R. G. *The Physics of Rubber Elasticity*, 3rd ed., Clarendon Press: Oxford, England, 1975.
(25) (a) Mooney, M. *J. Appl. Phys.* **1948**, *19*, 434. (b) Rivlin, R. S. *Philos. Trans. R. Soc. London, Ser. A* **1948**, *241*, 379.
(26) Ronca, G.; Allegra, G. *J. Chem. Phys.* **1975**, *63*, 4990.
(27) Flory, P. J. *Proc. R. Soc. London, Ser. A* **1976**, *351*, 351.
(28) LLorente, M. A.; Andrady, A. L.; Mark, J. E. *J. Polym. Sci.* **1980**, *18*, 2263−2270.
(29) Mark, J. E.; Rahalkar, R. R.; Sullivan, J. L. *J. Chem. Phys.* **1979**, *70*, 1794.
(30) James, H.; Guth, E. *J. Chem. Phys.* **1947**, *15*, 669.
(31) James, H.; Guth, E. *J. Chem. Phys.* **1951**, *19*, 1435.
(32) Tang, M. Y.; Mark, J. E. *Macromolecules* **1984**, *17*, 2616−2619.
(33) Zang, Y. H. Thesis, Université Louis Pasteur, Strasbourg, France, 1987.
(34) Zang, Y. H.; Muller, R.; Froelich, D. *J. Rheol.* **1986**, *30*, 1165.
(35) Muller, R.; Froelich, D.; Zang, Y. H. *J. Polym. Sci. Polym. Phys.* **1987**, *25*, 295.
(36) de Gennes, P.-G. *Scaling Concepts in Polymer Physics*; Cornell University Press: Ithaca, NY, 1979.
(37) Debye, P.; Bueche, A. M. *J. Appl. Phys.* **1949**, *20*, 518.
(38) Debye, P.; Anderson, H. R., Jr.; Brumberger, J. *J. Appl. Phys.* **1957**, *28*, 679.
(39) Landau, L. D.; Lifshitz, E. M. *Theory of Elasticity*; Pergamon Press: Oxford, England, 1986.
(40) Fredrickson, G. H.; Helfand, E. H. *Phys. Rev. Lett.* **1989**, *62*, 2468.
(41) Onuki, A. *J. Phys. Soc. Jpn.* **1989**, *58*, 3065.
(42) Poirier, C.; Ammi, M.; Bideau, D.; Troadec, J. P. *Phys. Rev. Lett.* **1992**, *68*, 216.
(43) Tanaka, T.; Hocker, L. O.; Benedek, G. B. *J. Chem. Phys.* **1973**, *59*, 5151.
(44) Onuki, A. Instabilities and Patterns in Elastic Materials: Gels and Solid Solutions. In *Formation, Dynamics, and Statistics of Patterns*; Kawasaki, K., et al., Eds.; World Scientific: Singapore, 1990.
(45) Rabin, Y.; Onuki, A. *Macromolecules* **1994**, *27*, 870.
(46) Stauffer, D. *Introduction to Percolation Theory*; Taylor and Francis: London, 1985.
(47) Daoud, M.; Leibler, L. *Macromolecules* **1988**, *21*, 1497.
(48) We consider a high concentrate polymer solution randomly cross-linked, the connectivity between the chains does not modify the correlations, and the percolation approach remains applicable. The shape of the scattering intensity is not changed and the random clusters so formed are invisible in the preparation state. Therefore, the clusters behave as *fractal objects* with a fractal dimension $D_p = 2.5$. The size distribution of the clusters is given by the power law: $p(M) \sim M^{-\tau}\exp(-M/M^*)$ where M^* is the high molecular weight. The polydispersity parameter τ is related to D_p (in three dimension, $\tau = 2.2$). The swelling of the system with a solvent reveal these clusters of different sizes. The solvent separates them and expels the clusters which screen their intercorrelations. Consequently, the fractal dimension of each cluster $D_p = 2.5$ due to the excluded volume effects is modified to $D_f = 2$ according to Flory arguments (a balance between the mixing and the elastic energies).
(49) Geissler, E.; Horkay, F.; Hecht, A. M. *Phys. Rev. Lett.* **1993**, *71*, 645.
(50) Rouf-George, C.; Munch, J. P.; Beinert, G.; Isel, F.; Pouchelon, A.; Palierne, J. F.; Boué, F.; Bastide, J. To be published.
(51) Gottlieb, M. Private discussion.
(52) Bastide, J. Thesis, Université Louis Pasteur, Strasbourg, France, 1984.
(53) Rouf-George, C.; Bastide, J.; Pujol, J. M.; Schosseler, F.; Munch, J. P. *Phys. Rev. Lett.* **1994**, *73*, 830.
(54) Straube, E.; Urban, V.; Pyckhout-Hintzen, W.; Richter, D.; Glinka, C. J. *Phys. Rev. Lett.* **1995**, *74*, 4464.
(55) Rabin, Y.; Panyukov, S. V. To be published.

MA961309Z